High *k*-Space Lasing in a Dual Wavelength Quantum Cascade Laser

Kale J. Franz*[1,a], Stefan Menzel*[1,2], Anthony J. Hoffman[1], Dan Wasserman[1,3], John W. Cockburn[2], and Claire Gmachl[1]

[1] Department of Electrical Engineering, Princeton University, Princeton, NJ 08544 USA
[2] Department of Physics and Astronomy, University of Sheffield, Sheffield, S3 7RH, UK
[3] Current address: Department of Physics, University of Massachusetts, Lowell, MA 01854 USA
[a] Email address: kfranz@princeton.edu
* Authors contributed equally

The understanding of charge carrier distributions is fundamental to our knowledge of laser systems. For example, charge carriers must generally achieve an inverted population profile between a high energy state and low energy state for optical amplification[1,2]. In semiconductor lasers, because of the charge carriers' propensity for extremely fast momentum relaxation[3,4], charge carriers accumulate at band extrema—i.e., have small wave vector near $k \approx 0$ in direct gap semiconductors. Conventional wisdom thus holds that the device-level physics happens at these band extrema, including population inversion for lasing. This behaviour is universal among diode lasers[5,6], unipolar interband quantum well lasers[7], and quantum cascade (QC) lasers[8,9]. An exception is present in hot-hole (p-Ge) lasers[10,11], where crossed electric and magnetic fields create local ($k \neq 0$) inversion between light and heavy hole bands in bulk semiconductor. Here, we report on a QC laser structure with an energy configuration able to establish local population inversion of electrons high in *k*-space through intrinsic processes. We observe dual wavelength emission from two discrete optical transitions. Temperature-dependent performance attributes show that the two transitions are highly coupled: competition for charge carriers is apparent from anti-correlated behaviour. The two optical transitions represent a conventional QC laser transition at $k \approx 0$ and another laser transition from non-thermal electrons at $k \approx 3.6\times10^{8}$ m^{-1}.

Inventing new semiconductor lasers has fundamentally relied on methods for obtaining population inversion. For example, the first QC lasers[8] sought to maximize inversion despite compromising oscillator strength; they used substantially spatially-delocalized energy states

populated with quasi-equilibrium electrons. Other, less traditional, methods have also been used to realize semiconductor injection lasers. Laser transitions with one state being a virtual state have been demonstrated both through Bloch gain[12,13] and stimulated Raman scattering[14]. Even here though, inversion is achieved from electron populations in quasi-equilibrium and thermally distributed around the Γ-point.

Hot-hole lasers diverge from the standard semiconductor laser configuration. The combination of large crossed electric and magnetic fields preferentially populates the light hole band by trapping electrons in cyclotron orbits at high *k*-space, while the applied electric field sweeps holes out of the heavy hole band through streaming motion[15]. Once these streaming holes in the heavy hole band reach the energy of an optical phonon, a scattering path opens where they can then repopulate the light hole band.

In the work presented here, instead of using externally applied electric and magnetic fields, we employ intrinsic scattering processes—i.e. the momentum transfer associated with optical phonons—to populate an energy subband high in *k*-space. Thermally distributed quasi-equilibrium electrons are injected into a lower energy subband at high *k*-space values. Population inversion for these "hot" electrons is achieved through the particulars of intra- and intersubband scattering.

The high *k*-space lasing reported here was discovered in an excited state QC laser[16]. Excited state QC lasers are characterized in that the primary optical transition is engineered to be between energy states that both have the quantum mechanical attributes of constituent quantum well excited states (e.g., at least one wavefunction node per coupled quantum well), while other QC lasers to-date have used optical transitions engineered from first-excited state to ground state transitions. In our two-well active region design, the primary transition is between a constituent quantum well second-excited state and first-excited state, labelled |5> and |4> respectively in the Fig. 1(a) conduction band energy diagram. This transition has a design energy of 128 meV (λ =

9.7 μm). A result of using excited state optical transitions is that additional lower-lying energy levels are inherently present in the structure. Three active region energy levels lie below the states of the |5>→|4> optical transition. With electron injection high in the active region structure, these other levels are candidates for supporting additional optical transitions.

We observe two distinct optical transitions in the spontaneous emission spectrum: one at $\lambda \approx 9.5$ μm and one at 8.2 μm, as shown in Fig. 1(b) for devices at 80 K. With ridge laser structures at 80 K, we find that these transitions lase simultaneously; similar threshold currents are observed at this temperature. We have previously identified[16] the 9.5 μm emission as originating from transition |5>→|4> and the 8.2 μm emission originating from transition |4>→|2>, based on the resonant wavelengths of the emission spectrum and the unique field-dependent behaviour of the optical emission.

A complete investigation of the temperature and current dependence of the emission reveals that each of the two transitions has distinctive temperature-dependent characteristics. Light from the |5>→|4> transition shows a behaviour typical of a QC laser intersubband optical transition. The highest output power and lowest threshold currents are achieved at low temperatures, as indicated in Figs. 2(a) and 2(c). As temperature increases, shorter non-radiative transition times, thermal population of the lower laser state, thermal emission from the upper laser state, and decreased upper laser level injection efficiency make obtaining population inversion more difficult to obtain. Consequently stronger pumping is required to achieve laser action, until a temperature is reached where the laser is unable to achieve threshold, in this case near 115 K.[17]

The lower |4>→|2> transition, however, deviates from the familiar intersubband optical transition behaviour significantly. Most strikingly, the transition lases more effectively at elevated temperatures (near 100 K), while performance is significantly diminished at lower temperatures. As shown in Figs. 2(b) and 2(c), lasing onset is thermally induced near 60 K. Peak output power with constant current density *increases* with temperature up to 115 K, while threshold current simultaneously *decreases*. For temperatures above 115 K, a thermal roll-over in

power is observed. The light-current curves in Fig. 2(d) reveal more: a threshold "crossover" is observed at 85 K, above which point the |4>→|2> transition develops a lower threshold than the |5>→|4> transition. At temperatures below this crossover, if the |4>→|2> transition is lasing, the |5>→|4> transition is also lasing. After the crossover and for low pumping rates, a regime exists where only the lower |4>→|2> transition lases. However, as soon as the upper |5>→|4> transition reaches threshold, an abrupt drop in |4>→|2> output power is observed. This anti-correlation in output power between the two transitions persists even above threshold. The Fig. 3(a) plot of thresholds shows that after crossover, the |4>→|2> transition threshold takes on a typical QC laser behaviour, having a characteristic temperature $T_0 \approx 220$ K; before crossover, however, the transition has a *negative* characteristic temperature $T_0 \approx -64$ K. The sharp "kink" in the |4>→|2> transition threshold at the crossover point along with the anti-correlated output power behaviour are indicative of the strong interaction between the carrier populations of the two optical transitions.

We used standard laser rate equations with stimulated emission terms to model a system with two optical transitions, including temperature-dependent parameters where appropriate. The models show that population inversion for the |4>→|2> transition is not feasible with a practical parameter set for a purely stacked transition scheme where both transitions lase from the Γ point ($k = 0$). Sequential transitions would also prohibit the observed anti-correlated behaviour; here, stronger |5>→|4> population inversion would lead to stronger |4>→|2> population inversion, contrary to what is observed. The data instead directly lead to a scheme whereby a second optical transition is in competition with a first transition for charge carriers. In a QC structure such as ours, we arrive at the model schematically depicted in Fig. 3(b); the second laser transition is a vertical transition between subbands, positioned high in *k*-space. Given the three identified energy subbands |5>, |4>, and |2>, several different electron transport paths are possible; two are labelled *A* and *B*. Path *A* is characteristic for a QC laser optical transition, where electrons undergo a radiative transition followed by longitudinal optical (LO) phonon scattering. When the

|5>→|4> transition is lasing, cavity photon densities at 9.5 μm and strong stimulated emission ensure that this is the dominant electron path. However, at elevated temperatures, path *B* becomes available with increased LO phonon scattering out of state |5>, populating state |4> high in *k*-space,[18] in this case near $k = 3.6\times10^8$ m^{-1}. If threshold has not yet been reached for the |5>→|4> transition, lasing can then occur at high *k*-space for the |4>→|2> transition. If at any time path *A* turns on, path *B* and therefore |4>→|2> population inversion is suppressed because (*i*) fewer electrons are available to populate the upper state of the high *k*-space |4>→|2> optical transition and (*ii*) electrons are injected into the lower state of the high *k*-space |4>→|2> transition. The observed anti-correlated behaviour of the two transitions is thus sustained.

That |4>→|2> population inversion can be achieved high in *k*-space may not be immediately obvious, given ultra-fast intrasubband relaxation dynamics. However, it is exactly these ultra-fast processes coupled with the non-parabolic nature[18,19] of energy states high in *k*-space that allow for high *k*-space population inversion in our QC structure. At the Brillouin zone centre k=0, energy subbands have a substantially parabolic form. However, with both increasing *k* and increasing subband energy above the band edge, the subbands flatten[20]. Thus the energy conversion of a ~34 meV LO phonon requires the exchange of a larger wave vector *k* for higher energy subbands, which in turn reduces the scattering rate[3,21,22] as $1/k^2$ (Refs. 23,24). This makes it possible to obtain a longer non-radiative intrasubband relaxation time for the |4>→|2> upper laser state than for the lower laser state at high *k*, as required for population inversion. Using the $1/k^2$ dependence, we calculate the intrasubband scattering times at $k = 3.6\times10^8$ m^{-1} for states |4> and |2> to be related by $\tau_{4k}/\tau_{2k} = 2.2$. Furthermore, the intrasubband scattering processes are faster than their intersubband counterparts: high *k*-space population inversion in subband |4> is not forbidden by lower-energy active and injector region subbands into which state |4> electrons can non-radiatively scatter. In this way, only local[25] *k*-space population inversion is achieved, while global population inversion is not required.

Our rate equation model thus includes seven energy "levels": five for each of the active region energy levels labelled in Fig. 1(a) and two high *k*-space regions for subbands |4> and |2>. The temperature dependence of energy state lifetimes[9], gain[26], injection efficiency, thermal backfilling of energy states[9], and thermionic emission[27] were all included. Figure 3(a) illustrates how the model is able to accurately reproduce three key features of the observed data: (*i*) the unconventional threshold behaviour of the |4>→|2> laser transition that decreases then increases with temperature; (*ii*) the crossing of the |5>→|4> and |4>→|2> laser thresholds; and (*iii*) the sharp kink in the temperature-dependent evolution of the |4>→|2> transition threshold at the crossover point.

In conclusion, we have demonstrated a dual wavelength QC structure that lases with one conventional ($\lambda \approx 9.5$ μm) and one high *k*-space ($\lambda \approx 8.2$ μm) optical transition. The QC laser shows dual wavelength emission, with the high *k*-space transition being anti-correlated with the primary, excited state laser transition. A rate equation model based on incorporating a high *k*-space optical transition reproduces characteristic features of the observed temperature-dependent emission behaviour. The demonstration of *k*-space lasing represents a departure from the conventional approaches to semiconductor lasers, presenting the possibility of designing intersubband devices making more cognizant use of full *k*-space population distributions.

Methods

Laser Growth and Fabrication

The laser was grown using gas source molecular beam epitaxy on an InP substrate. The active core contains 40 periods of the layer sequence (in angstroms starting from the injection barrier) **32**/98/**13**/86/**13**/35/**10**/35/**10**/20/**16**/27/**16**/20/**19**/16/**23**/23, where $In_{0.52}Al_{0.48}As$ barrier layers are in bold, $In_{0.53}Ga_{0.47}As$ well layers are in normal font, and Si-doped (2×10^{17} cm^{-3}) layers are underlined. The active core was embedded in a conventional dielectric, InP-based waveguide. Full details of the device fabrication can be found in Ref. 16.

Measurements and Characterization

Spectra shown in Fig. 1(a) were collected using a Fourier transform infrared (FTIR) spectrometer with 100 ns current pulses at 50 kHz. The temperature-dependent light-current (LI) measurements of Fig. 2 were taken with 100 ns current pulses at 5 kHz using a gated integrator and boxcar averager. A long pass filter with cut-off at $\lambda = 8.65$ μm and a short pass filter with cut-off at $\lambda = 8.70$ μm were used to spectrally resolve emission from the two transitions. For a thorough study of the structure, along with preliminary characterization of multiple (~30) laser devices, we performed full, detailed, temperature-dependent characterizations on five different lasers from different parts of the wafer. Cavity lengths were 1.38, 1.48, 1.50, 1.63, and 2.28 mm. All devices showed similar anti-correlated behaviour between two competing optical transitions lasing near $\lambda \approx 9.5$ μm and 8.2 μm. In all cases, a stronger $|5\rangle \rightarrow |4\rangle$ transition always led to a weaker $|4\rangle \rightarrow |2\rangle$ transition. The data shown in the main text result from the 1.48 mm device.

References

[1] Siegman, Anthony E., *Lasers*. (University Science Books, Sausalito, CA, 1986).

[2] Yariv, Amnon, *Quantum Electronics*, 3rd ed. (Wiley, New York, 1989).

[3] Alcalde, A. M. and Weber, G., Nonparabolicity effects on electron-optical-phonon scattering rates in quantum wells. *Phys. Rev. B* **56** 9619 (1997).

[4] Rudin, S. and Reinecke, T. L., Electron LO-phonon scattering rates in semiconductor quantum wells. *Phys. Rev. B* **41** 7713 (1990).

[5] Kroemer, Herbert, Nobel Lecture: Quasielectric fields and band offsets: teaching electrons new tricks. *Rev. Mod. Phys.* **73** 783 (2001).

[6] Alferov, Zhores I., Nobel Lecture: The double heterostructure concept and its applications in physics, electronics, and technology. *Rev. Mod. Phys.* **73** 767 (2001).

[7] Olafsen, L. J., Vurgaftman, I., and Meyer, J. R., in *Long-wavelength Infared Semiconductor Lasers*, edited by H. K. Choi (Wiley, Hoboken, NJ, 2004).

[8] Faist, J. et al., Quantum Cascade Laser. *Science* **264** 553 (1994).

[9] Gmachl, C., Capasso, F., Sivco, D. L., and Cho, A. Y., Recent progress in quantum cascade lasers and applications. *Rep. Prog. Phys.* **64** 1533 (2001).

[10] Shastin, V.N., Hot hole inter-sub-band transition p-Ge FIR laser. *Opt. Quantum Electron.* **23** S111 (1991).

[11] Bründermann, E., in *Long-wavelength Infared Semiconductor Lasers*, edited by H. K. Choi (Wiley, Hoboken, NJ, 2004).

[12] Terazzi, R. et al., Bloch gain in quantum cascade lasers. *Nature Physics* **3** 329 (2007).

[13] Revin, D. G. et al., Dispersive gain and loss in midinfrared quantum cascade laser. *Appl. Phys. Lett.* **92** 081110 (2008).

[14] Troccoli, M. et al., Raman injection laser. *Nature* **433** 845 (2005).

[15] Pinson, W. E. and Bray, R., Experimental determination of the energy distribution functions and analysis of the energy-loss mechanisms of hot carriers in p-type germanium. *Physical Review* **136** A1449 (1964).

[16] Franz, K. J. et al., Evidence of cascaded emission in a dual-wavelength quantum cascade laser. *Appl. Phys. Lett.* **90** 091104 (2007).

[17] While QC lasers routinely surpass room temperature operation, high thermal performance is not expected in this case due to the proximity of state |5> to the barrier band edge and the associated thermally induced current leakage.

[18] Serapiglia, G. B., Vodopyanov, K. L., and Phillips, C. C., Nonequilibrium electron distributions in a three-subband InGaAs/InAlAs quantum well studied via double resonance spectroscopy. *Appl. Phys. Lett.* **77** 857 (2000).

[19] Dirisu, Afusat O. et al., *to be submitted*.

[20] Sirtori, C., Capasso, F., Faist, J., and Scandolo, S., Nonparabolicity and a Sum-Rule Associated With Bound-to-Bound and Bound-to-Continuum Intersubband Transitions in Quantum-Wells. *Phys. Rev. B* **50** 8663 (1994).

[21] Ridley, B. K., *Quantum Processes in Semiconductors*, 4 ed. (Oxford University Press Inc., New York, 1999).

[22] Sinning, S. et al., Reduced subpicosecond electron relaxation in GaNxAs1-x. *Appl. Phys. Lett.* **86** (2005).

[23] Bockelmann, U. and Bastard, G., Phonon scattering and energy relaxation in two-, one-, and zero-dimensional electron gases. *Phys. Rev. B* **42** 8947 (1990).

[24] Harrison, P., *Quantum Wells, Wires and Dots: Theoretical and Computational Physics of Semiconductor Nanostructures*, 2 ed. (Wiley, 2005).

[25] Faist, J. et al., Quantum cascade lasers without intersubband population inversion. *Phys. Rev. Lett.* **76** 411 (1996).

[26] Faist, J. et al., in *Semiconductors and Semimetals*, edited by H. C. Liu and F. Capasso (Academic Press, 2000), Vol. 66, pp. 36.

[27] Sze, S., *Physics of Semiconductor Devices*. (John Wiley and Sons, Inc., New York, 1981).

Acknowledgements

We gratefully acknowledge helpful comments, advice, and support from Stephen R. Forrest, Kuen-Ting Shiu, and Ines Waldmueller. This work was supported in part by MIRTHE (NSF-ERC #EEC-0540832) and the European Marie Curie Research Training Network POISE. K.J.F. gratefully acknowledges the support of the NSF Graduate Research Fellowship Program.

Correspondence should be addressed to K.J.F.

Figure 1 **Excited state QC laser band diagram and emission spectra** (a) A portion of the conduction band energy diagram for our QC structure, composed of interleaved $Al_{0.48}In_{0.52}As$ barriers and $In_{0.53}Ga_{0.47}As$ quantum well layers. The conduction band edge is shown at an applied electric field E = 72 kV/cm. The quantized subband energies and the associated wave functions (squared moduli) are also shown. Five key active region subbands are labelled, with optical transitions identified as |5>→|4> and |4>→|2>, and indicated by red and blue wavy arrows, respectively. The transition between states |5> and |4> represents a second-excited state to first-excited state transition. The |4>→|2> optical transition occurs high in k-space, as is shown later in Fig. 3(b). (b) Emission spectra for one QC laser at a heat sink temperature of 80 K. Electroluminescence is followed by laser action as the applied electric field and pumping current are increased. We identify transition |5>→|4> as the source of the $\lambda \approx 9.5$ μm emission and transition |4>→|2> as the source of the 8.2 μm emission.

Figure 2 **Light output characteristics of a representative device** Light output versus current density and heat sink temperature for the (a) ~9.5 μm and (b) ~8.2 μm light. Data shown for the transition |5>→|4> ~9.5 μm light are consistent with standard QC laser behaviour; i.e., lower threshold current densities and higher output powers are observed for lower heat sink temperatures. In contrast, the |4>→|2> transition operates poorly at the lowest heat sink temperatures; the transition instead has thermally-induced peak performance near a heat sink temperature $T \approx 115$ K. With the |5>→|4> transition threshold (white circles) overlaid on (b), one sees that the |4>→|2> transition power roll-off is coincident with |5>→|4> turn-on. (c) Spectrally-resolved light output for three fixed pumping current densities with increasing temperature. The |5>→|4> transition is shown with dashed lines, and the |4>→|2> transition is shown with solid lines. The |4>→|2> transition output is affected by the |5>→|4> transition output power. (d) Light-current curves for each optical transition at 80 K and 105 K. A "crossover" in laser thresholds occurs at 85 K, where the |4>→|2> transition achieves a lower

threshold than the |5>→|4> transition. At 105 K, transition |4>→|2> has the lower threshold; here, the |5>→|4> transition threshold marks the beginning of the |4>→|2> power roll-off. The inset shows current-voltage curves for 6.5 and 155 K heat sink temperatures.

Figure 3 **Model results and *k*-space representation** (a) Observed and modelled temperature-dependent threshold current densities for the two optical transitions. Red circles indicate thresholds for the |5>→|4> ~9.5 μm transition, and blue circles represent the |4>→|2> ~8.2 μm light. A crossover in thresholds is seen near 85 K. Prior to this crossover, the |4>→|2> transition threshold decreases with increasing temperature. A sharp "kink" is observed in the |4>→|2> threshold when it becomes lower than that of transition |5>→|4>. These features are reproducible with a conventional QC rate-equation model with temperature-dependent parameters[26], the results of which are indicated by dashed lines. (b) A schematic representation of the high *k*-space lasing. The *k*-space dispersion of the subbands |5>, |4>, and |2> is shown. Electrons, being injected into state |5>, can follow either path *A* (the |5>→|4> optical transition) or path *B* (the |4>→|2> optical transition preceded by LO phonon scattering). Path *A* is typical for a QC laser transition, while path *B* represents the high *k*-space transition. Optical transitions are indicated by wavy arrows, intersubband phonon transitions are shown with dashed-line arrows, intrasubband scattering is shown with curved arrows, and paths *A* and *B* are shown with dotted arrows.

Figure 1

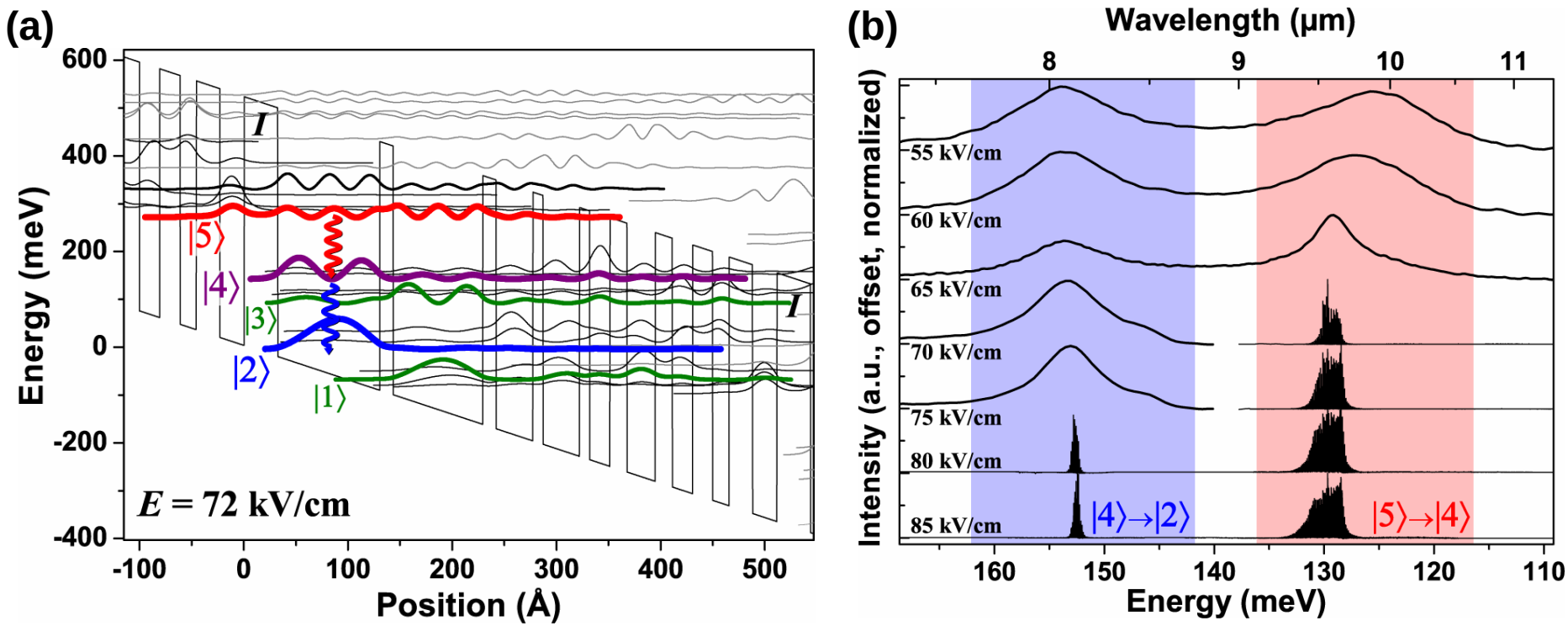
(a)
Energy (meV)
Position (Å)
E = 72 kV/cm
|5⟩
|4⟩
|3⟩
|2⟩
|1⟩
I
I
(b)
Wavelength (μm)
Intensity (a.u., offset, normalized)
Energy (meV)
55 kV/cm
60 kV/cm
65 kV/cm
70 kV/cm
75 kV/cm
80 kV/cm
85 kV/cm
|4⟩→|2⟩
|5⟩→|4⟩

Figure 2

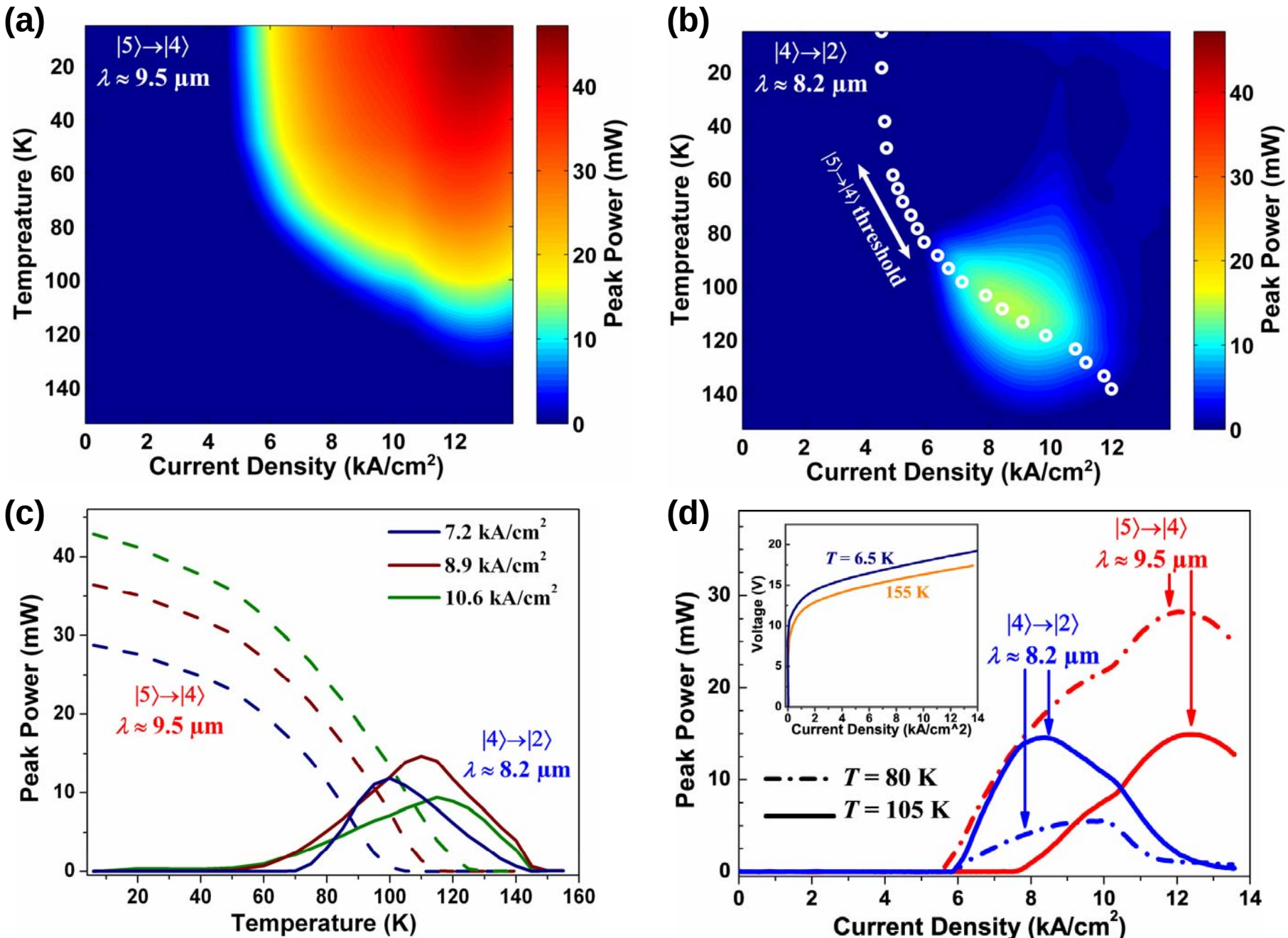
(a)
|5⟩→|4⟩
λ ≈ 9.5 μm
Tempreature (K)
Current Density (kA/cm²)
Peak Power (mW)
(b)
|4⟩→|2⟩
λ ≈ 8.2 μm
|5⟩→|4⟩ threshold
Tempreature (K)
Current Density (kA/cm²)
Peak Power (mW)
(c)
7.2 kA/cm²
8.9 kA/cm²
10.6 kA/cm²
|5⟩→|4⟩
λ ≈ 9.5 μm
|4⟩→|2⟩
λ ≈ 8.2 μm
Peak Power (mW)
Temperature (K)
(d)
T = 6.5 K
155 K
Voltage (V)
Current Density (kA/cm^2)
|5⟩→|4⟩
λ ≈ 9.5 μm
|4⟩→|2⟩
λ ≈ 8.2 μm
T = 80 K
T = 105 K
Peak Power (mW)
Current Density (kA/cm²)

Figure 3

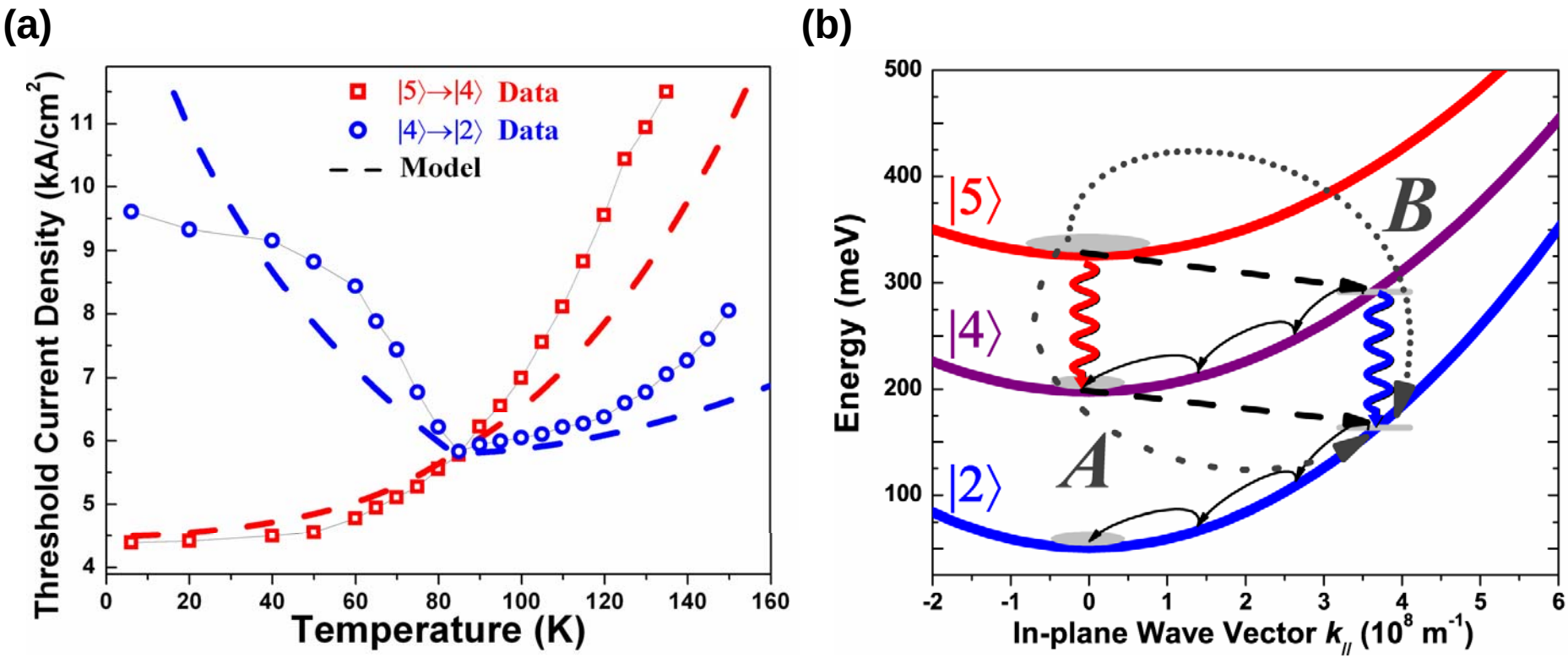
(a)
|5⟩→|4⟩ Data
|4⟩→|2⟩ Data
Model
Threshold Current Density (kA/cm²)
Temperature (K)
(b)
|5⟩
|4⟩
|2⟩
B
A
Energy (meV)
In-plane Wave Vector k// (10⁸ m⁻¹)